Cluster Chemistry

Deutsche Ausgabe: DOI: 10.1002/ange.201604269
Internationale Ausgabe: DOI: 10.1002/anie.201604269

# Controlling the Adsorption of Carbon Monoxide on Platinum Clusters by Dopant-Induced Electronic Structure Modification

*Piero Ferrari, Luis M. Molina,* Vladimir E. Kaydashev, Julio A. Alonso, Peter Lievens, and Ewald Janssens**

***Abstract:*** *A major drawback of state-of-the-art proton exchange membrane fuel cells is the CO poisoning of platinum catalysts. It is known that CO poisoning is reduced if platinum alloys are used, but the underlying mechanism therefore is still under debate. We study the influence of dopant atoms on the CO adsorption on small platinum clusters using mass spectrometry experiments and density functional calculations. A significant reduction in the reactivity for Nb- and Mo-doped clusters is attributed to electron transfer from those highly coordinated dopants to the Pt atoms and the concomitant lower CO binding energies. On the other hand Sn and Ag dopants have a lower Pt coordination and have a limited effect on the CO adsorption. Analysis of the density of states demonstrates a correlation of dopant-induced changes in the electronic structure with the enhanced tolerance to CO poisoning.*

The development of efficient fuel cells is a promising strategy to diminish the dependence on fossil fuel by making use of environmentally friendly energy sources.[1] Proton exchange membrane fuel cells (PEMFCs) are highly susceptible to CO poisoning of the platinum catalyst.[2] CO molecules, present as trace components in the fuel, preferentially adsorb on Pt nanoparticles, thereby blocking the active sites and degrading the performance of the cell. Several Pt alloys, such as Pt-$X$ ($X$ = Sn, Ru, Mo, Nb, W, Ag, and Ni), are known for an enhanced tolerance to the CO poisoning and thus improve the performance of the fuel cell.[3–7] The physical mechanism responsible for the tolerance has been extensively studied and is ascribed to an alteration of the local electronic structure at the reaction site upon alloying and/or to a bifunctional mechanism, in which OH groups adsorbed on the alloying agent interact with CO and form $CO_2$ and $H_2$, which are released from the catalyst, regenerating the active sites.[3]

The interaction of transition-metal surfaces with CO is a complex problem which has been described by three qualitative models: the d-band center model,[8] the Blyholder model,[9] and the π-σ model.[10] In the Blyholder model, the Pt–CO interaction is described by donation of electron density from the CO 5σ orbital to the empty Pt 5d states and back-donation from occupied Pt 5d states to the CO 2π* antibonding orbital. The bottom line of local electronic structure modifications as explanation for the CO tolerance in Pt-$X$ alloy nanoparticles is that electron transfer from the alloying agent to the empty Pt 5d states reduces the Pt–CO bonding strength.[11]

Although few-atom platinum clusters in the gas phase differ significantly in size and in environmental conditions from the nanoparticles used in PEMFCs, they can provide a better understanding for the enhanced tolerance to CO poisoning. The CO binding is a local event, which poisons a Pt active site. Clusters in molecular beams are ideal model systems for complex processes that depend on local chemistry. Conditions (cluster size, composition, and charge state) are well controlled in a gas-phase experiment. In addition, reactions with unknown molecules are excluded if the experiments are performed under high vacuum conditions while the small size of the clusters allows for direct comparison with quantum-chemical calculations.[12,13] For instance, studies on the small $Pd_6^+$ cluster identified the $Pd_6O_4^+$ oxide as a key intermediate in the catalytic combustion of CO.[14] Joined experimental and theoretical studies on $V_xO_y^+$ clusters elucidated the nature of the active site in the catalytic ethylene oxidation on vanadium oxide,[15] and experiments on $Au_2^+$ clusters demonstrated the activation of methane on Au with subsequent release of ethylene.[16]

Here we combine mass spectrometric experiments and DFT calculations to study the influence of dopant atoms on the CO adsorption on small Pt clusters. The size-selected clusters are ideal model systems to investigate how doping modifies the local electronic structure at the active Pt site, thereby altering the CO adsorption strength. At the same time, the experimental high-vacuum conditions eliminate the presence of bifunctional mechanisms.[17]

Cationic doped Pt clusters, $XPt_n^+$ ($X$ = Mo, Nb, Sn, and Ag; $13 \le n \le 23$), are produced in a dual-target dual-laser vaporization source. The room-temperature clusters are subsequently exposed to CO gas in a low-collision reaction cell and the abundances of the cluster–CO complexes are analyzed by time-of-flight mass spectrometry.[18] With the

[*] P. Ferrari, Dr. V. E. Kaydashev, Prof. Dr. P. Lievens, Prof. Dr. E. Janssens
Laboratory of Solid State Physics and Magnetism, KU Leuven
Celestijnenlaan 200d, Box 2414, 3001 Leuven (Belgium)
E-mail: ewald.janssens@fys.kuleuven.be
Prof. Dr. L. M. Molina, Prof. Dr. J. A. Alonso
Department of Theoretical, Atomic and Optical Physics
Universidad de Valladolid
Paseo Belén 7, 47011 Valladolid (Spain)
E-mail: lmolina@fta.uva.es
Dr. V. E. Kaydashev
Current address:
Laboratory of Nanomaterials, Southern Federal University
344090 Rostov-on-Don (Russia)
Supporting information and the ORCID identification number(s) for the author(s) of this article can be found under http://dx.doi.org/10.1002/anie.201604269.

  

used CO pressures ($p_{CO} \leq 0.05$ Pa) up to two CO molecules are adsorbed on the clusters.

A part of the mass spectrum of pure and Nb-doped Pt clusters, recorded for a CO pressure of 0.05 Pa in the collision cell, is presented in Figure 1 a. For all bare $Pt_n^+$ clusters,

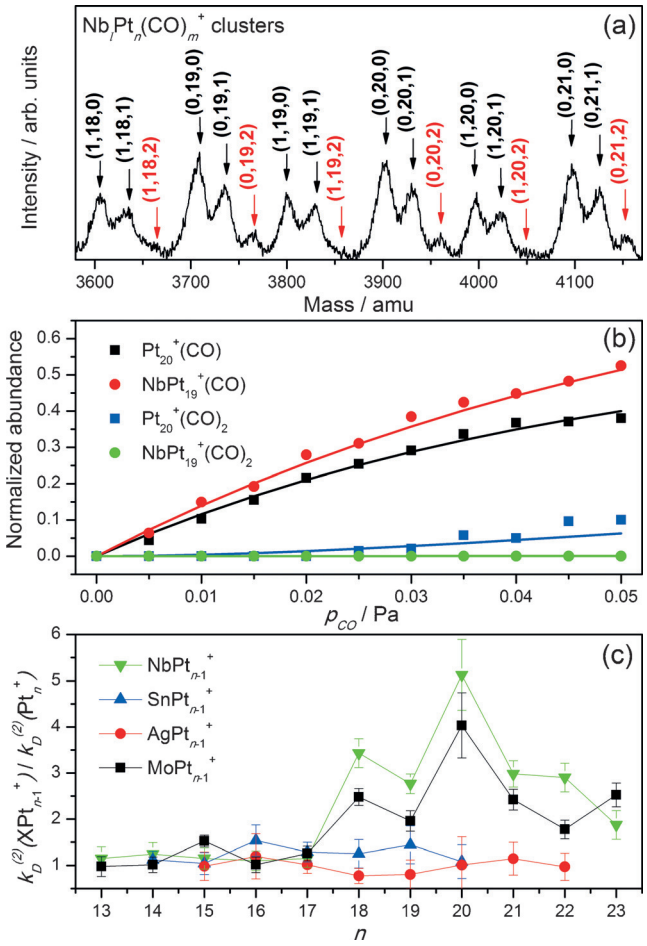


***Figure 1.*** a) Part of the mass spectrum of pure and Nb-doped Pt clusters exposed to 0.05 Pa of CO gas. The label (*l*,*n*,*m*) refers to the composition of the complexes Nb$_l$Pt$_n$(CO)$_m^+$. (CO)$_2$ complexes are marked in red. b) Fit of normalized intensities of (CO) and (CO)$_2$ complexes of $Pt_{20}^+$ and $NbPt_{19}^+$ clusters as a function of $p_{CO}$. c) Size dependence of the ratio of backward reaction coefficients $k_D^{(2)}$ of doped to pure Pt clusters.

complexes with one and two CO molecules are formed, while for the doped $NbPt_{n-1}^+$ ($n = 18$–22) clusters the intensity of the complexes with two CO molecules is low. This clearly illustrates the influence of Nb doping on the likelihood for CO adsorption. The molecular beam of clusters interacts with CO in the collision cell and formed complexes are mass-analyzed about 100 μs later, corresponding to the flight time from the cell to the extraction zone of the mass spectrometer. The influence of the Nb dopant is mainly reflected on the adsorption of the second CO molecule and in the $n = 18$–22 size range, which is a consequence of the time scale of the experiment and is explained below.

Figure 1 b illustrates the pressure-dependent kinetics data, which reveal an increase in the cluster-(CO) and cluster-(CO)$_2$ complexes with $p_{CO}$. The formation of cluster-CO complexes can be described by a two-step reaction mechanism, characterized by forward ($k_f^{(1,2)}$) and backward ($k_D^{(1,2)}$) reaction coefficients for adsorption and desorption of the first (1) and second (2) CO molecule [Eqs. (1) and (2)],[18]

$$Pt_n^+ + 2\,CO \underset{k_D^{(1)}}{\overset{k_f^{(1)}}{\rightleftharpoons}} Pt_n(CO)^+ + CO \underset{k_D^{(2)}}{\overset{k_f^{(2)}}{\rightleftharpoons}} Pt_n(CO)_2^+ \quad (1)$$

$$Pt_n(CO)_2^+ \xrightarrow{k_D^{(2)}} Pt_n(CO)^+ + CO \xrightarrow{k_D^{(1)}} Pt_n^+ + CO \quad (2)$$

where (1) and (2) represent the reaction mechanism for clusters in and after the reaction cell.

The fits presented in Figure 1 b show that $k_f^{(1)}$ and $k_f^{(2)}$ can be approximated by hard-sphere collision rates, while the size- and dopant-dependent strength of the cluster–(CO)$_{1,2}$ bonds is reflected in the magnitude of $k_D^{(1,2)}$.[19] A detailed description of this procedure and the validity of the underlying analysis is presented as Supporting Information.

The dependence of the unimolecular dissociation rates on the CO adsorption energies can be simulated with statistical RRKM analysis (see the Supporting Information). Desorption rates of the first CO molecule, $k_D^{(1)}$, are found slower than the time scale of the experiment. This explains why size and dopant dependences are only seen in the desorption of the second CO molecule. $k_D^{(2)}$ is significantly higher than $k_D^{(1)}$, because the corresponding clusters are internally heated by adsorption of two instead of one CO molecule. For example, assuming binding energies of 2.4 eV and 2.0 eV for the first and second CO molecule on $Pt_{19}^+$ (energies are taken from the DFT calculations in the Supporting Information), the simulated value of $k_D^{(2)}$ is $6 \times 10^3\ s^{-1}$. A dopant induced reduction of the adsorption energies by 0.4 eV results in an increase of $k_D^{(2)}$ to about $10^7\ s^{-1}$. Such a high $k_D^{(2)}$ implies dissociation before detection and thus a strong reduction in the measured abundance of the doped cluster–(CO)$_2$ complex.

Because of the finite size of the heat bath, $k_D^{(1,2)}$ strongly depends on the size of the cluster. In a small cluster, with few degrees of freedom, the same CO adsorption energy results in a large temperature increase and thus a high unimolecular dissociation rate.[17] For example, no cluster–(CO)$_2$ complexes are observed for clusters with less than 17 atoms, since they all dissociate on the time scale of the experiment. Also this observation can be well explained by the RRKM simulations (see the Supporting Information).

Figure 1 c presents the ratio of the fitted dissociation rates $k_D^{(2)}$ for the doped clusters (with $X$ = Mo, Nb, Sn, and Ag) to that of pure Pt clusters as a function of cluster size. Comparing clusters of the same size one can make abstraction of the heat bath effect on the dissociation rates and directly probe the influence of the dopant atom. It is remarkable that $k_D^{(2)}$ is not significantly affected by the substitution of Pt for Sn or Ag dopants ($k_D^{(2)}$ ratio in Figure 1 c is around unity), while doping with Mo or Nb leads to a strong increase in $k_D^{(2)}$ for $n > 17$ cluster sizes. This different behavior in terms of CO binding energies will be described further.

DFT was used to analyze the chemical bonding of CO with representative $Pt_{19}^+$ and $XPt_{18}^+$ ($X$ = Nb, Mo, Ag, and Sn) clusters. Simulations were carried out within the projector augmented-wave method as implemented in the GPAW software using a 20 Å cubic cell.[20,21] The spacing of the real-space 3D grid was set to 0.2 Å and exchange-correlation effects were modelled with the Perdew–Burke–Ernzerhof exchange-correlation functional.[22,23] The self-consistent field convergence threshold was set to $10^{-6}$ eV/e$^-$. Structure optimization was carried out using the Broyden–Fletcher–Goldfarb–Shanno (Quasi-Newton) algorithm until forces were below 0.01 eV Å$^{-1}$.

The lowest energy structural isomer found for $Pt_{19}^+$ has an octahedral shape, which has also been predicted computationally for neutral $Pt_{19}$.[24] Isomers for $XPt_{18}^+$ are explored by substituting inequivalent sites of $Pt_{19}^+$ with the dopant atom, followed by local structural optimization. The obtained minimum energy structures are shown in Figure 2. Nb and

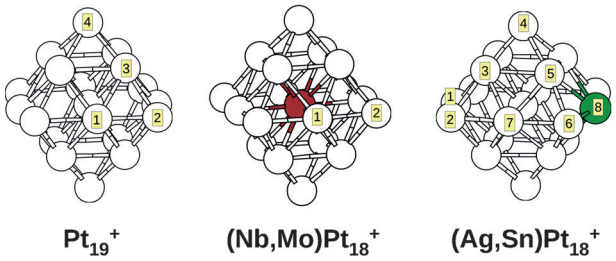


***Figure 2.*** Relaxed structures of $Pt_{19}^+$ and $XPt_{18}^+$ clusters ($X$ = Nb, Mo, Ag, and Sn). Dopant atoms are colored in red (Nb, Mo) and green (Ag, Sn). Inequivalent surface sites are numbered.

Mo preferentially locate at the cluster core, whereas Ag and Sn occupy an edge site. CO adsorption energies, are calculated for adsorption of CO to each inequivalent surface site. The largest CO adsorption energies (Table 1) are

***Table 1:*** Calculated CO adsorption energies and Bader charges on $X$ in $XPt_{18}^+$ clusters.

| Cluster | $E_{ads}$ [eV] | Bader charge |
|---|---|---|
| $Pt_{19}^+$ | −2.38 | – |
| $NbPt_{18}^+$ | −1.81 | +1.73 |
| $MoPt_{18}^+$ | −1.83 | +1.40 |
| $AgPt_{18}^+$ | −2.26 | +0.37 |
| $SnPt_{18}^+$ | −2.21 | +0.95 |

obtained at edge site (1) for both the $Pt_{19}^+$ and all $XPt_{18}^+$ clusters [$E_{ads} = E_{cluster\text{-}CO} - (E_{cluster} + E_{CO})$].

The CO binds most strongly with pure $Pt_{19}^+$ ($E_{ads}$ = 2.38 eV), while a much weaker CO binding is found for Nb- and Mo-doped Pt clusters ($E_{ads} \approx 1.8$ eV). The values for Ag- and Sn-doped clusters ($E_{ads} \approx 2.2$ eV) are close to that of pure Pt. The calculated lower CO binding energy for Nb- and Mo-doped Pt clusters is in good agreement with the mass spectrometric observations. As shown in the RRKM analysis (see the Supporting Information) a reduction in the CO binding energy considerably increases the cluster–CO dissociation rates, which is reflected in lower abundances of cluster–$(CO)_2$ complexes. The DFT result that Ag and Sn doping only slightly reduces $E_{ads}$ also agrees with the experimental data, since for these dopants no significant change in cluster reactivity was observed.

Figure 3 presents an analysis of the clusters' electronic structures. The upper panel shows the total DOS of $Pt_{19}^+$ and

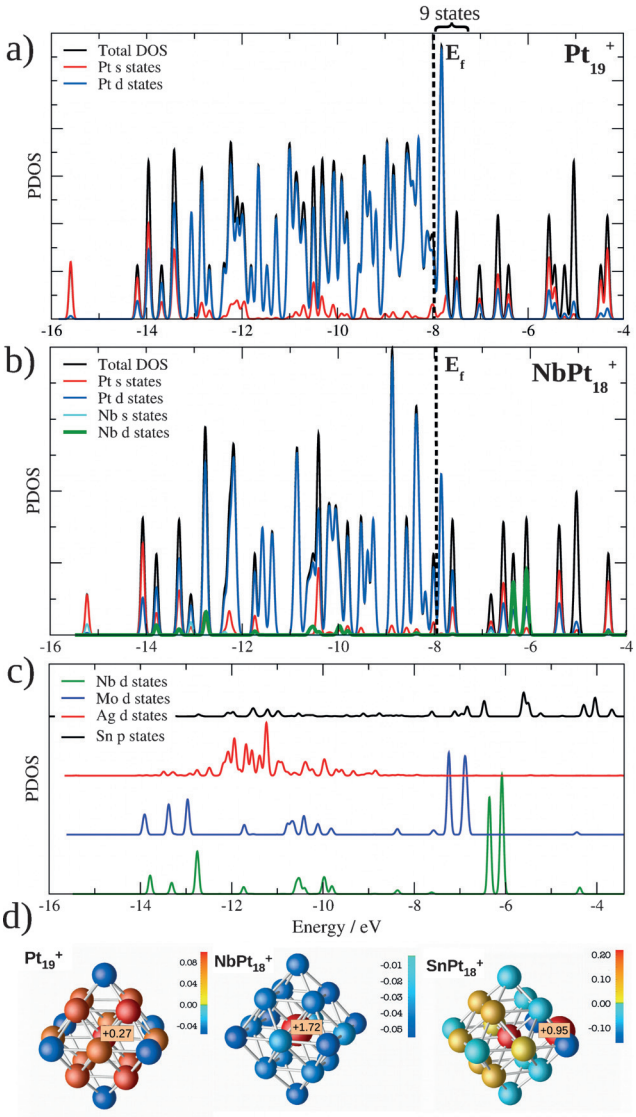


***Figure 3.*** Total and projected densities of states (DOS) for a) $Pt_{19}^+$ and b) $NbPt_{18}^+$ clusters. c) Series of projected DOS into the d states of the impurity atom (p states for Sn) for $XPt_{18}^+$ clusters. d) Bader charges on $Pt_{19}^+$, $NbPt_{18}^+$, and $SnPt_{18}^+$. Positively (negatively) charged atoms are colored with various shades of red (blue). Labels indicate the value of charges which lie off the scale. The dopant atoms have a larger size.

projections into atomic Pt s and d states. As expected, the electronic structure is dominated by valence d states, which form a band ranging from −14 to −7.5 eV. This d band is nearly full, with only nine empty states from the Fermi level, $E_F$, to the top of the band.

Figure 3b shows an analogous DOS analysis for $NbPt_{18}^+$, including projections on s and d states of Nb. Most of the Nb d states are located above the Fermi level. Nb d electrons are transferred to the Pt d band. Hereby, $E_F$ moves up slightly, with only seven empty states from $E_F$ to the top of the valence band. A comparison of the valence occupancy of the different dopants in $XPt_{18}^+$ is presented in Figure 3c. For heavier dopants the electronegativity difference between dopant and Pt gets smaller and the energy of the dopant's d states decreases. Nb has the largest dopant–host charge transfer, followed by Mo, while most of the Ag d states have energies within the Pt d band. Sn dopants are qualitatively different, as charge transfer takes place from 5p orbitals. The Sn 5p orbitals are located partly inside, and partly outside the Pt d band.

A Bader charge analysis demonstrates dopant-induced charge transfer. Figure 3d illustrates that the charge in pure $Pt_{19}^+$ is distributed over edge-like sites (around +0.09 e at each site) and the central atom (+0.27 e), while there is a very large net positive charge on the central dopant atom in $NbPt_{18}^+$ (+1.73 e) and all Pt atoms are negatively charged. The Mo dopant in $MoPt_{18}^+$ has also a large, however slightly lower, net positive charge (see Table 1). In contrast, charge transfer from Ag to the Pt cluster is much smaller. In $SnPt_{18}^+$ there mainly is charge transfer from the edge located Sn dopant to the neighboring Pt atoms, while other Pt edge sites still have a positive charge. Overall, the Bader charge of the Pt atoms is strongly correlated with CO adsorption energies, with a stronger CO bonding at sites with a more positive charge (see Supporting Information for CO binding energies at different sites). The smaller CO binding energy on $NbPt_{18}^+$ and $MoPt_{18}^+$ can thus be rationalized by the large charge transfer from the dopants to all Pt atoms of the clusters. In $AgPt_{18}^+$ and $SnPt_{18}^+$ CO preferentially binds on Pt atoms distant from the dopant that are positively charged.

Figure 4 provides a detailed analysis of the cluster–CO bond. There is a strong interaction between the 5σ orbital, which is strongly shifted down in energy, and the Pt d states. In addition, hybridization between the 2π MO and the d states results in levels with partially 2π character below the Fermi energy. Also the CO 1π orbitals hybridize with Pt states. The shapes of charge redistributions upon bonding confirm a major role of donation from σ orbitals, which becomes more difficult when the Pt reaction sites are negatively charged.

In summary, a combined mass spectrometric and density functional theory study has shown that a single dopant atom in small cationic Pt clusters alters the interaction strength of the clusters with CO. The magnitude of the effect depends on the kind of dopant atom, with a significant change in the cluster–CO interaction upon Nb and Mo doping and no or minor influence for Sn and Ag doping. The Nb and Mo dopants occupy highly coordinated positions in the clusters concomitant with a large dopant-Pt charge transfer, thereby affecting the local electronic structure of all Pt atoms including the CO reaction site. This is not the case for Sn and Ag, which take low coordinated positions in the Pt clusters. The higher occupancy of the Pt valence d band in Nb- and Mo-doped clusters is responsible for the reduced CO adsorption energies, which explains the lower abundances of the cluster–$(CO)_2$ complexes in the experiment.

Several Pt alloy nanoparticles, including PtNb, PtMo, PtSn and PtAg, have been tested in real PEMFCs and show an improved tolerance to CO poisoning. We demonstrated the particular role of intraparticle charge transfer on the CO binding energies in Pt clusters containing a single dopant atom. Since CO binding is a local event, conclusions from this work may be relevant for larger Pt-*X* alloy nanoparticles that show enhanced CO tolerance and should be considered when developing future fuel cells with better durability.

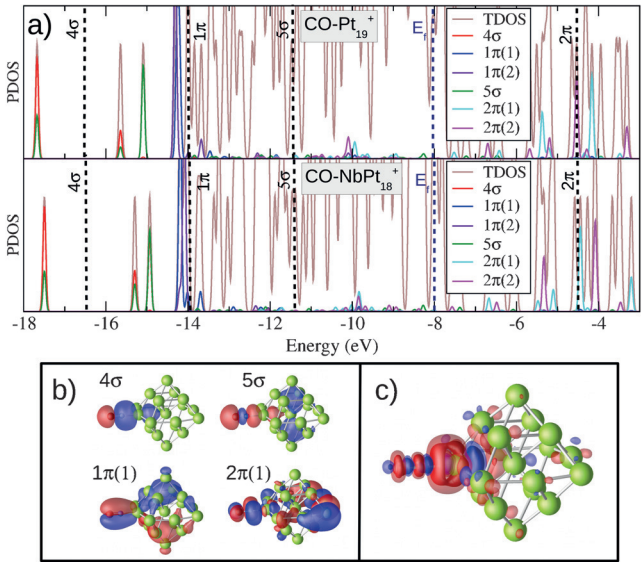


***Figure 4.*** a) Projected densities of states (PDOS) on the CO molecular orbitals (MO) for CO-$Pt_{19}^+$ and CO-$NbPt_{18}^+$. The gray line shows total DOS. Dashed vertical lines indicate the position of free CO MOs. b) Wave functions of selected CO related states on CO-$Pt_{19}^+$. c) Plot of induced charge density differences for CO-$Pt_{19}^+$. Red/blue contours represent regions of charge accumulation/depletion, respectively.

## Acknowledgements

This work is supported by the Research Foundation-Flanders (FWO) and by the KU Leuven Research Council (GOA/14/007). P.F. acknowledges CONICyT for Becas Chile scholarship. The work in Valladolid was supported by MINECO (grant number MAT2014-54378-R) and Junta de Castilla *y* Leon (grant number VA050U14).

**Keywords:** carbon monoxide · clusters · density functional calculations · kinetics · mass spectrometry

**How to cite:** *Angew. Chem. Int. Ed.* **2016**, *55*, 11059–11063
*Angew. Chem.* **2016**, *128*, 11225–11229

[1] X. Zhao, M. Yin, L. Ma, L. Liang, C. Liu, J. Liao, T. Lu, W. Xing, *Energy Environ. Sci.* **2011**, *4*, 2736.
[2] J. Baschuk, X. Li, *Int. J. Energy Res.* **2001**, *25*, 695.
[3] S. Ehteshamia, S. Chan, *Electrochim. Acta* **2013**, *93*, 334.
[4] Y. Feng, L. Bi, Z. Liu, D. Kong, Z. Yu, *J. Catal.* **2012**, *290*, 18.

[5] J. Hu, Z. Liu, B. Eichhorn, G. Jackson, *Int. J. Hydrogen Energy* **2012**, *37*, 11268.
[6] J. Kim, S. Choi, S. Nam, M. Seo, S. Choi, W. Kim, *Appl. Catal. B* **2008**, *82*, 89.
[7] T. Rocha, F. Ibanhi, F. Colmati, J. Linares, V. Paganin, E. Gonzalez, *J. Appl. Electrochem.* **2013**, *43*, 817.
[8] J. K. Nørskov, T. Bligaard, J. Rossmeisl, C. H. Christensen, *Nat. Chem.* **2009**, *1*, 37.
[9] G. Blyholder, *J. Chem. Phys.* **1964**, *68*, 2772.
[10] N. Dimakis, M. Cowan, G. Hanson, E. S. Smotkin, *J. Phys. Chem. C* **2009**, *113*, 18730.
[11] M. Liao, C. Cabrera, Y. Ishikawa, *Surf. Sci.* **2000**, *445*, 267.
[12] H. Schwarz, *Angew. Chem. Int. Ed.* **2015**, *54*, 10090; *Angew. Chem.* **2015**, *127*, 10228.
[13] S. Zhou, J. Li, M. Schlangen, H. Schwarz, *Acc. Chem. Res.* **2016**, *49*, 494.
[14] S. M. Lang, I. Fleischer, T. M. Bernhardt, R. N. Barnett, U. Landman, *J. Am. Chem. Soc.* **2012**, *134*, 20654.
[15] D. Justes, R. Mitrić, N. Moore, V. Bonačić-Koutecký, A. Castleman, Jr., *J. Am. Chem. Soc.* **2003**, *125*, 6289.
[16] S. M. Lang, T. Bernhardt, R. Barnett, U. Landman, *Angew. Chem. Int. Ed.* **2010**, *49*, 980; *Angew. Chem.* **2010**, *122*, 993.
[17] V. Kaydashev, E. Janssens, P. Lievens, *Int. J. Mass Spectrom.* **2015**, *379*, 133.
[18] H. Le, S. M. Lang, J. De Haeck, P. Lievens, E. Janssens, *Phys. Chem. Chem. Phys.* **2012**, *14*, 9350.
[19] E. Janssens, H. T. Le, P. Lievens, *Chem. Eur. J.* **2015**, *21*, 15256.
[20] J. Mortensen, L. Hansen, K. Jacobsen, *Phys. Rev. B* **2005**, *71*, 035109.
[21] J. Enkovaara, et al., *J. Phys.: Condens. Matter* **2010**, *22*, 253202.
[22] J. Perdew, K. Burke, M. Ernzerhof, *Phys. Rev. Lett.* **1996**, *77*, 3865.
[23] M. Marques, M. Oliveira, T. Burnus, *Comput. Phys. Commun.* **2012**, *183*, 2272.
[24] L. Xiao, L. Wang, *J. Chem. Phys.* **2004**, *108*, 8605.

Received: May 2, 2016
Revised: June 13, 2016
Published online: July 28, 2016

  